

**ASSESSMENT OF AIRBORNE PARTICULATE
MATTER AND RADIOACTIVITY AT QASSIM,
SAUDI ARABIA**

ALNAGRAN HAMED MOHAMMED O

UNIVERSITI SAINS MALAYSIA

2023

**ASSESSMENT OF AIRBORNE PARTICULATE
MATTER AND RADIOACTIVITY AT QASSIM,
SAUDI ARABIA**

by

ALNAGRAN HAMED MOHAMMED O

**Thesis submitted in fulfilment of the requirements
for the degree of
Doctor of Philosophy**

September 2023

ACKNOWLEDGEMENT

Despite the fact that my name appears on the cover of this work, several others have contributed, and I am grateful to all who have helped make this study possible. My heartfelt thanks go to my supervisor, Dr. Nursakinah Suardi. She allowed me the opportunity to explore on my own while also providing me with outstanding advice, encouragement, and support during my study and never-ending support. This work would never have been feasible without her expertise and encouragement. I felt so grateful to have her as my advisor. I wish to express my sincere appreciation to the co-supervisor, Dr. Azhar Abdul Rahman, for his assistance and support. I would like to acknowledge the members of my committee for taking an interest in my work, reviewing my dissertation, and giving constructive feedback. I would like to thank all members of the technical resources at Qassim University for their assistance during the lab experiments. I appreciate Dr. Mohammed Alshitawi, president of Mustaqbal University for his support. I would like to offer my special thanks to Dr. Howaida Mansour and Dr. Abid Albadri for their assistance with the chemistry lab. Also, I would like to extend my sincere thanks to Professor Bassam Abdulrahman for helping with the nuclear physics lab. I want to express my heartfelt gratitude to my parents and my wife, Rawan Alqother, for their unwavering support during my studies and research at Universiti Sains Malaysia. Finally, financial support from Qassim University (QU) is gratefully acknowledged.

TABLE OF CONTENTS

ACKNOWLEDGEMENT	ii
LIST OF TABLES	vii
LIST OF FIGURES	ix
LIST OF SYMBOLS	xix
LIST OF ABBREVIATIONS	xxv
ABSTRAK	xxix
ABSTRACT	xxxii
CHAPTER 1 INTRODUCTION	1
1.1 Overview	1
1.2 Scope of work	4
1.3 Problem Statement	6
1.4 Objectives of the research	7
1.5 Outline of thesis	7
CHAPTER 2 LITERATURE REVIEW	8
2.1 Particulate Matter on urban environment.....	8
2.1.1 Categories of particulate matter	10
2.1.1.(a) Primary particulate matter	12
2.1.1.(b) Secondary particulate matter	12
2.1.2 Airborne particulate matter physical characteristics	13
2.1.2.(a) Normal and Logarithmic Normal Distributions	17

2.1.2.(b)	Shape of particulate matter	20
2.1.3	Airborne particulate matter chemical characteristics	20
2.1.4	Transportation of airborne particulate matter	27
2.1.5	The damaging effects of PM on health	30
2.2	Radionuclides and Radioactive Pollutants	32
2.3	Background of CFD Modelling	33
2.4	CFD Modelling	38
2.4.1	Forces on a single particle.....	38
2.4.2	Turbulence.....	41
2.5	Background of Filtration	43
2.6	Filtration.....	46
2.6.1	Filtration of PM.....	46
2.6.2	Outdoor filtration	47
2.6.3	Filter clogging	50
2.7	Theory of Filtration	50
2.7.1	Single fiber Efficiency theory	50
2.8	Permeodynamic filtration technology (PFT)	54
2.9	Total annual air filtration costs	56
CHAPTER 3	MATERIALS AND METHOD	58
3.1	Materials, equipment and software	58
3.1.1	PM sampling tolls	58
3.1.2	Mixer and rotator device	59
3.1.3	PM Monitoring equipment.....	59

3.1.3.(a)	Accuracy	61
3.1.4	X-ray fluorescence analyzer.....	61
3.1.5	X-ray diffraction analyzer	63
3.1.6	Scintillator detector	64
3.1.7	3.1.7 SolidWorks simulation software.....	65
3.1.8	The media filter (Energyflo™ Cell).....	65
3.1.9	Air velocity transducer device	66
3.2	Methodology	67
3.3	Site description.....	68
3.4	Monitoring of PM	71
3.5	Chemical analysis.....	73
3.5.1	Enrichment Factor	75
3.6	Statistical measurements	75
3.6.1	The measured activity	75
3.6.2	Radiological parameters.....	76
3.7	Methodology for conducting CFD simulations.....	78
3.7.1	CFD Simulation Model.....	78
3.7.2	Computational domain	80
3.7.3	Particulate matter pollution studies.....	82
3.7.4	Boundary Conditions (B.C)	83
3.7.5	Governing equations	88
3.7.6	Mesh sensitivity analysis.....	92
3.7.7	Laboratory model	99
3.7.8	Objective of lab modelling.....	99

3.7.9	Approach	101
3.8	Methodology for Air filtration	108
3.8.1	Filter design and laboratory plant	108
3.8.2	Field trial setup.....	111
3.8.3	Measurement and calculation of PM efficiency.....	112
3.8.4	Pressure drop measurement.....	116
CHAPTER 4	RESULT AND DISCUSSION	117
4.1	Physical analysis results.....	117
4.2	Chemical analysis results	122
4.3	Radioactivity analysis results.....	132
4.3.1	Assessments radiological risk hazard.....	132
4.4	Simulation of PM dispersion in an urban environment	143
4.4.1	Validation of model.....	144
4.5	Air filtration results	160
4.5.1	Laboratory-based test results.....	160
4.5.2	Field trial results.....	174
4.5.3	Comparison between outdoor air filters.....	181
4.5.4	Uniformity of air flow	182
CHAPTER 5	CONCLUSION AND FUTURE WORK.....	185
	REFERENCES.....	190
	APPENDICES	
	LIST OF PUBLICATION	

LIST OF TABLES

	Page
Table 2.1	Airborne PM chemicals (percentages) worldwide (Harrison and Yin, 2000).25
Table 2.2	PM mass concentration and chemical composition in Europe by type of site (Putaud et al., 2010).26
Table 3.1	Locations of the samples collected.74
Table 3.2	Commutational domain size.82
Table 3.3	The characteristics of the media filter.110
Table 3.4	Characteristic of two filter media.....113
Table 3.5	Air cleaners specifications (area cross section: 0.25 mm × 2000 mm).115
Table 4.1	Statistical criteria of the concentration of the PM for one year (urban).117
Table 4.2	Statistical criteria of the concentration of the PM for one year (rural).118
Table 4.3	Comparison of Average PM concentration in different locations.120
Table 4.4	Chemical abundances of deposition sample.123
Table 4.5	Chemical compound of deposition samples.....124

Table 4.6	Comparison of the EF with the regional and global weighted averages.	128
Table 4.7	Activity concentration and standard deviation of Ra-226, Th-232 and K-40 (Bq/Kg) radium equivalent, the external (Hex) and internal hazard index (Hin) and level index (Iy).	133
Table 4.8	Comparison of the hazard index with some selected studies.	134
Table 4.9	Environment hazard index for investigated samples.	137
Table 4.10	Distribution correlation between radionuclides.	140
Table 4.11	Comparison values of activity concentration (Bq/kg) of natural radionuclides with reported from different countries of the world.	140
Table 4.12	Calculated mean efficiency of filtration at different air flow rates.	161
Table 4.13	Pressure drop over time.....	162
Table 4.14	A comparison between different types of outdoor air filters.	181
Table 4.15	Uniformity of air velocity inside the test rig.....	184

LIST OF FIGURES

	Page
Figure 2.1	Size comparisons for PM particles (USEPA, 2022)..... 14
Figure 2.2	Schematic display of the distribution of PM size in ambient air (USEPA, 1996). 16
Figure 2.3	Log-normal distribution plotted in log space (a) with parameters $N_0 = 1$, $\mu = -1$ and $\sigma = 0.4$ and linear space (b); The distribution mode, median and mean in log and linear space, respectively (Grainger, 2012). 19
Figure 2.4	Schematic view of a cross street with people-regarding particulate air pollution (Mosler, 2014). 30
Figure 2.5	Schematic diagram of movement into and around the metropolitan environment (Grimmond and Oke, 1999). 35
Figure 2.6	Effects of St number on particle dispersion (Crowe et al., 2011)... 42
Figure 2.7	Predicted fibre collection region (Hinds, 1999). 51
Figure 2.8	Collection mechanisms for single fibre: interception, diffusion and impaction (Sutherland, 2011). 53
Figure 3.1	(a) The real PM collection in the field, (b) Diagram showing the PM collection tool..... 58
Figure 3.2	Device for homogenising samples..... 59

Figure 3.3	Optical particle counter 1.108 (Grimm Aerosol Technik GmbH & Co. KG, 2012).....	59
Figure 3.4	Laser measuring chamber series 1.108 (Grimm Aerosol Technik GmbH & Co. KG, 2012).....	60
Figure 3.5	The ARL Quant'X (Thermo Scientific Inc., USA) EDXRF.....	62
Figure 3.6	Rigaku, UK, X-Ray Ultima IV Diffractometer.	64
Figure 3.7	Scintillator detector NaI (Tl).	65
Figure 3.8	Cell of Energyflo™: 50 mm Energyflo cell, 20 mm air gap and 10 mm plasterboard with vent in both sides, (L: 60 cm × W: 60 cm). 66	
Figure 3.9	Air Velocity Transducer 8475 series (TSI Incorporated, 2020).	67
Figure 3.10	Flowchart of the methodology.....	68
Figure 3.11	Map of Qassim at the centre of Saudi Arabia from (Google maps, 2022).	69
Figure 3.12	High temperature and low temperature daily in Qassim (Weatherspark, 2019).	70
Figure 3.13	The average annual wind patterns in Qassim (Weatherspark, 2019).	70
Figure 3.14	Average humidity in Qassim (Worldweatheronline, 2019).....	71
Figure 3.15	PM monitoring sites in Qassim region (Google maps, 2023)..	72

Figure 3.16	Geologic map of studied PM in Qassim region (Alnagran et al., 2022)	74
Figure 3.17	Design of the simulation model for Union Street and King Street (1240 m × 740 m).	79
Figure 3.18	Flow Simulation Wizard approach.	80
Figure 3.19	Computational domain for the Union Street and King Street model.	82
Figure 3.20	The computational domain for CFD simulation (Blocken et al., 2007).	84
Figure 3.21	Resolution domain and boundary.	85
Figure 3.22	Wind speed profile for boundary condition (Blocken et al., 2007).	88
Figure 3.23	Three main types of fluid cell based on the geometry of the assembly (SolidWorks technical reference, 2014).	93
Figure 3.24	Meshing process (Basic mesh, Initial mesh and Final mesh) (SolidWorks technical reference, 2014).	95
Figure 3.25	The slider bar progressively refines the mesh from levels 1–8.	97
Figure 3.26	The shape of meshing in the model.	98
Figure 3.27	Number of cells or grids.	98

Figure 3.28	The structure of the three-dimensional model (laboratory plant). 100
Figure 3.29	Model Dimensions (Plan View).102
Figure 3.30	(a) Inlet flow rate of the filter, (b) outlet flow rate of the filter, (c) nebulize flow rate.104
Figure 3.31	The fitted mesh of the model.106
Figure 3.32	Partial cell in the simplest case and two control volumes (CV) (Sobachkin et al., 2013).106
Figure 3.33	Post-refinement SolidWorks Flow Simulation mesh (Sobachkin et al., 2013).107
Figure 3.34	(a) Permeodynamic filter test rig and air flow schematics in the lab, (b) The real filter in the lab, (c) The lab schematics.110
Figure 3.35	Permeodynamic filter test rig for field trial.111
Figure 3.36	Maps for outdoor trials in Qassim University (Google Maps, 2022).112
Figure 3.37	Scanning electron microscope (SEM) images for (a) Synthetic-depth filter, (b) Energyflo™ cells- depth filter and (c) surface filter.112
Figure 3.38	Theoretical efficiencies results for Energyflo™ cells filter.113
Figure 3.39	Theoretical efficiency of aerosol particle collection mechanisms for a fibrous filter. These measurements were based on ‘single-fibre

	efficiency' for filters, as discussed in more detail in Hinds (1999). Image has been adapted from Hinds (1999).	114
Figure 3.40	Effect of fibre diameter on pressure drop and efficiency (Imbabi and Peacock, 2004).	114
Figure 3.41	Schematic diagram of the pressure drop test apparatus.	116
Figure 3.42	Evolution of pressure drop with time (Imbabi and Peacock, 2004).	116
Figure 4.1	(a) PM ₁₀ , (b) PM _{2.5} , (c) PM ₁ concentration in urban and rural areas of Qassim. (d) The peak of PM, which indicates the disparity between day and night readings.	119
Figure 4.2	Comparisons of PM ₁₀ concentration in urban and rural areas.	121
Figure 4.3	Comparison of PM _{2.5} concentrations in urban and rural areas.	122
Figure 4.4	Chemical concentration of deposition samples (elements).	124
Figure 4.5	Chemical concentration of deposition samples (chemical compound).	125
Figure 4.6	Chemical compound as minerals (%).	130
Figure 4.7	Measurement profile of sample 1 (S1).	131
Figure 4.8	Activity concentration (Bq/kg) for ²²⁶ Ra, ²³² Th and ⁴⁰ K for whole samples from different locations.	133

Figure 4.9	The relative contribution to absorbed dose for ^{226}Ra , ^{232}Th and ^{40}K	134
Figure 4.10	The external and internal hazards in addition to gamma level index for investigated 276 samples.	135
Figure 4.11	Radium equivalent (Bq/kg) against dose rate (nGy/h).	138
Figure 4.12	The relation between dose rate (nGy/h) and annual effective dose ($\mu\text{Sv/y}$).	138
Figure 4.13	Correlation between Ra-226 and Th-232 (Bq/kg).	141
Figure 4.14	Correlation between Ra-226 and K-40 (Bq/kg).	141
Figure 4.15	Correlation between Th-232 and K-40 (Bq/kg).	142
Figure 4.16	Flow streamlines (flow trajectories of PM) for different wind directions: (a) north, (b) south (c) east (d) west respectively.	146
Figure 4.17	Cut off plots for velocity of PM from different wind directions: (a) north, (b) south (c) east (d) west respectively.	147
Figure 4.18	Cut off plots for PM mass fraction from different wind directions: (a) north, (b) south (c) east (d) west respectively.	148
Figure 4.19	Experimentally observed data of PM concentration as function of time.	150
Figure 4.20	Simulated result of PM concentration as a function of time.	150

Figure 4.21	Trajectory of flow during the operation of filter (a) before, (b) during and (c) after filtration.	152
Figure 4.22	Cut off plots before operation the filter.	153
Figure 4.23	Cut off plots 20 minutes of Air Cleaner Operation.	153
Figure 4.24	Cut off plots 40 minutes of Air Cleaner Operation.	154
Figure 4.25	Cut off plots of PM concentration during operation of filter.	155
Figure 4.26	Updated Path lines of aerosol.	156
Figure 4.27	Velocity flow field (side view).....	157
Figure 4.28	Velocity flow field (front view).....	157
Figure 4.29	Pressure drop vs time.....	163
Figure 4.30	PM concentration vs time for (a) PM ₁₀ , (b) PM _{2.5} , and (c) PM ₁ before and after filtration with an air flow rate of 10 m ³ /hr.	165
Figure 4.31	Cumulative PM concentration for PM ₁₀ , PM _{2.5} , and PM ₁ before and after filtration with an air flow rate of 10 m ³ /hr.	165
Figure 4.32	(a) Efficiency vs time for cumulative PM ₁₀ , PM _{2.5} , and PM ₁ ; (b) Efficiency for different size of PM from 0.3 to 20 μm with an air flow rate of 10 m ³ /hr.....	166
Figure 4.33	PM concentration vs time for (a) PM ₁₀ , (b) PM _{2.5} , and (c) PM ₁ before and after filtration with an air flow rate of 35 m ³ /hr.	167

Figure 4.34	Cumulative PM concentration of PM ₁₀ , PM _{2.5} , and PM ₁ before and after filtration with an air flow rate of 35 m ³ /hr.	168
Figure 4.35	(a) Efficiency vs time for cumulative PM ₁₀ , PM _{2.5} , and PM ₁ ; (b) Efficiency for different size of PM from 0.3 to 20 μm with an air flow rate of 35 m ³ /hr.	168
Figure 4.36	Cumulative PM concentration of PM ₁₀ , PM _{2.5} , and PM ₁ before and after filtration with an air flow rate of 35 m ³ /hr at ½ m from the test rig.	169
Figure 4.37	Efficiency vs time for cumulative PM ₁₀ , PM _{2.5} , and PM ₁ at ½ m from the test rig.	169
Figure 4.38	Cumulative PM concentration of PM ₁₀ , PM _{2.5} , and PM ₁ before and after filtration for an air flow rate 35 m ³ /hr at 1 m from the test rig.	170
Figure 4.39	Efficiency vs time for cumulative for PM ₁₀ , PM _{2.5} , and PM ₁ at 1 m from the test rig.	170
Figure 4.40	Cumulative PM concentration for PM ₁₀ , PM _{2.5} , and PM ₁ for air flow rate of 35 m ³ /hr at 2 m from the test rig.	171
Figure 4.41	Efficiency vs time for cumulative PM ₁₀ , PM _{2.5} , and PM ₁ at 2 m from the test rig.	171

Figure 4.42	Cumulative PM concentration of PM ₁₀ , PM _{2.5} , and PM ₁ before and after filtration for an air flow rate of 35 m ³ /hr at 3 m from the test rig.	172
Figure 4.43	Efficiency vs time for cumulative PM ₁₀ , PM _{2.5} , and PM ₁ at 3 m from the test rig.....	172
Figure 4.44	Cumulative PM concentration of PM ₁₀ , PM _{2.5} , and PM ₁ for an air flow rate of 35 m ³ /hr at 4 m from the test rig.	173
Figure 4.45	Efficiency vs time for cumulative PM ₁₀ , PM _{2.5} , and PM ₁ at 4 m from the test rig.....	173
Figure 4.46	Mean efficiency of filtration vs different air flow rates (depth filter).	176
Figure 4.47	Mean efficiency of filtration vs different air flow rates (surface filter).	176
Figure 4.48	PM concentration (upstream and downstream) of (a) PM ₁₀ , (b) PM _{2.5} , and (c) PM ₁ for an air flow rate of 100 m ³ /hr vs time, and (d) the efficiency for different size of PM from 0.3 to 20 μm (Depth Filter).	177
Figure 4.49	PM concentration of (a) PM ₁₀ , (b) PM _{2.5} , and (c) PM ₁ for an air flow rate of 1000 m ³ /hr at 1 m from the test rig (Depth Filter). ...	178

Figure 4.50	PM concentration of (a) PM ₁₀ , (b) PM _{2.5} , and (c) PM ₁ for an air flow rate of 400 m ³ /hr and (d) the efficiency for different size of PM from 0.3 to 20 μm (Surface filter).....	179
Figure 4.51	PM concentration of (a) PM ₁₀ , (b) PM _{2.5} , and (c) PM ₁ for an air flow rate of 1000 m ³ /hr at 1 m from the test rig (Surface Filter)..	180
Figure 4.52	Location of the 15th points.....	182
Figure 4.53	Air flow simulation inside the test rig. The blue colour illustrated that the air velocity is almost unchanged.....	183

LIST OF SYMBOLS

Greek letters

$\frac{\partial(\rho_g \phi)}{\partial t}$	the local acceleration expression (m/s ²)
u_g	the dynamic viscosity of the gas (Pa s)
\bar{u}	gas mean velocity (m/s)
v_g	the gas velocity (m/s)
v_p	the particle velocity (m/s)
η_R	interception efficiency (-)
$\mu_{g,t}$	the turbulent viscosity (P-s)
μ_g	Dynamic viscosity of the gas phase (Pa s)
ρ_g	gas density (kg/m ³)
ρ_p	particle density (kg/m ³)
σ_0	the standard deviation of the distribution
$\partial\Omega$	boundary condition (m)
f	scalar function (m)
I_γ	gamma level index (Sv)
m/Ω	area density of captured particles (kg/m ²)
u	the fluid velocity (m/s)
u'	gas fluctuating velocity (-)
v	the gas velocity (m/s)
α_p	volume of a particle phase (m ³)
α	the packing density of the filter (-)
α_f	packing density of the virgin filter (-)

α_p	packing density of the particles collected (-)
β	constant observed by measurement (-)
δ	the standard deviation (-)
δh	particular thickness (m)
δ_{ij}	the Kronecker delta function (-)
ε	turbulent dissipation rate (m^2/s^3)
ε'	photopeak efficiency
ε_g	turbulent kinetic energy dissipation rate (m^2/s^3).
$\eta_{f,j,l}$	the time-invariant single-fibre collection efficiency (sec)
η	the dynamic viscosity (Pa-s)
η_D	Brownian efficiency (-)
η_{im}	Impaction efficiency (-)
θ	angle of incidence or an angle of Bragg
λ	the mean free path (m)
μ	the dynamic viscosity (Pa-s)
μ_t	the turbulent eddy viscosity (m^2/s)
ρ	the fluid density (kg/m^3)
$\rho u'u'$	Reynolds stresses (-)
τ_g	time of flow scale (sec)
τ_{ij}	the viscous shear stress tensor (Pa)
ψ	stream function ($kg/m-s$)
Ω	field function (-)

Latin letters

F_D	drag force for Stokes' rule (N)
P_k	turbulent kinetic energy output rate (J/kg)
A	cross-sectional area of the filter; (m ²)
AGDR	absorbed gamma dose rate (nGy/h)
Bq/kg	activity of individual radionuclides (Bq)
C (²²⁶ Ra)	activity concentrations of ²²⁶ Ra (Bq/kg)
C (²³² Th)	activity concentrations of ²³² Th (Bq/kg)
C (⁴⁰ K)	activity concentrations of ⁴⁰ K (Bq/kg)
C ₁	represents a constant (3/4)
C _b	an air mass concentration (kg/m ³)
C _C	slip correction factor (-)
C _{in}	number concentration or the particle mass that enter the filter (kg/m ³)
C _o	the drag coefficient (-)
C _{out}	number concentration or the particle mass that leave the filter (kg/m ³)
C _T	the drag coefficient for virgin filters (-)
C _{Tm} (z,t)	the drag constant for fibers clogged with particles (-)
D	the measure of diffusion coefficient (m ² /s)
D	the molecular of the contaminant fluid (kg)
d	the perpendicular division of adjacent pairs of planes
df	the fiber diameter (m)
d _{fm}	diameter of a dust loaded fibre (m)
D _p	aerodynamic diameter, the diameter of unit density (μg)
d _p	the mean diameter of dendrites (m)
D _p	the particle diameter (m)

D^T	turbulent diffusive factors of the contaminant fluid (m^2/s)
Dz	specific thickness of layer (m)
E_d	Brownian diffusion of single fiber efficiency (-)
E_I	inertial impaction of single fiber efficiency (-)
E_R	interception of single fiber efficiency (-)
E_{Σ}	the single-fiber efficiency (-)
E_{Σ}	amount of SFE due to interception, inertial and Brownian diffusion (-)
f	drag factor
f_{μ}	damping function of Lam and Bremhorst (kg/s)
g_i	the factor of gravitational acceleration (m/s^2)
g_i	the gravitational acceleration component along the i-th coordinate direction (m/s^2)
H_{ex}	external hazards of RAD (Sv)
H_{in}	internal hazards of RAD (Sv)
k	the penetration factor of the filtration media (-)
k_g	the phase gas of turbulent kinetic energy (J/kg)
Kn	Knudsen number- ratio of particle size to mean free path (-)
Ku	Kuwabara number (-)
$L=$	length or diameter of the fluid (m)
L_f	the overall length of the fibres (m)
L_p	the whole length of dendrites in ($\mu m/m^2$)
L_s	characteristic length (m)
M	the mass of sample (kg)
m	the mean value of the air velocity (m/s)

m_{LF}	the coefficient that represents the mass of captured particles in every unit length of the fiber (kg/m)
m_p	the particle mass in the mixture's unit volume
n	the boundary surface unit normal if $\Omega \subset R$
N_o	Particle concentration (kg/m ³)
N_s/t_s	count per second for sample (-)
P	average fluid pressure (Pa)
P	the filter penetration (-)
P_0	pressure drop (Pa)
P_B	the turbulent generation due to buoyancy forces (N)
Q	the volumetric flow rate of particles (m ³)
q_i	the diffusive heat flux (W/m)
R	strain rate (s ⁻¹)
$Ra(eq)$	radium equivalent activity in (Bq/kg)
Re	Reynold numbers
R_f	Radius of fibre (m)
Si	a mass-distributed external force per unit mass (N/kg)
St	Stokes number
$V(h)$	means the speed of the wind at a particular height (m/s)
V_c	dimensional volume (m ³)
V_{Fibre}	volume of fibre (m ³)
V_{Filter}	volume of the filter (m ³)
V_r	speed at a reference height (m/s)
V_s	function velocity (m/s)
W	represents the ratio ($\Delta P/Q$) (Pa/m ³)

y	the distance from the wall (m)
z	the filter thickness (m)
ΔP	pressure drop (Pa)

LIST OF ABBREVIATIONS

AAS	atomic absorption spectrophotometry
Al	Aluminium
AQEG	Air Quality Expert Group
AQMS	Air Quality Monitoring Station
As	Arsenic
ASHRAE	American Society of Heating, Refrigerating and Air-Conditioning Engineers
AURN	Automatic Urban and Rural Network
Ba	Barium
Br	Bromine
Ca	Calcium
CAD	Computer-Aided Design
CFD	Computational Fluid Dynamic
Cl	Chlorine
CO ₂	Carbon Dioxide
COMEAP	Committee on the Medical Effects of Air Pollution
Cr	Chromium
Cu	Copper
EDS	Energy Dispersion Spectrometer
EDXRF	Energy-Dispersive X-Ray Fluorescence
EN	European Standard
Fe	Iron
HEPA	High-efficiency Particulate Air (filter)
IAEA	International Atomic Energy Agency

ICRP	International Commission on Radiological Protection
IPCC	Intergovernmental Panel on Climate Change
K	Potassium
K-40	Potassium-40
LAQI	Local Air Quality Index
Mg	Magnesium
Mn	Manganese
MOUDI	Micro-Orifice Deposit Impactor
Na	Sodium
NaI (TI)	Sodium iodide
NAS	National Academy of Science
NEA	Nuclear Energy Agency
NH	Nihonium
Ni	Nickel
NIST	National Institute of Standards and Technology
No	Nobelium
NR	Annealed Mineral
Pb	Lead
PFT	Permeodynamic Filtration Technology
PIXe	Proton-Induced X-ray emissions
PM, PMs	Particulate Matter
PM ₁	Particulate Matter less than 1 microns in aerodynamic diameter
PM ₁₀	Particulate Matter less than 10 microns in aerodynamic diameter
PM _{2.5}	Particulate Matter less than 2.5 microns in aerodynamic diameter
PM _{2.5-10}	Coarse Particles with Diameter between 2.5µm and 10µmCFD

ppb	parts per billion
ppm	parts per million
PSL	Poly-Styrene Latex
PTFE	Polytetrafluoroethylene (Teflon)
Q	Quartz
QUARG	Quality of Urban Air Review Group
Ra-226	Radium-226
RANS	Reynolds-Averaged Navier–Stokes
Rb	Rubidium
RNG	Re-Normalisation Group
SCHER	Scientific Committee on Health and Environmental Risks
SEM	Scanning Electron Microscopy
So	Sulfur
Sr	Strontium
SVF	Solid Volume Fraction
Th-232	Thorium-232
Ti	Titanium
TSPs	Total Suspended Particles
U-238	Uranium-238
UCC	Upper Continental Crust
UNSCEAR	United Nations Scientific Committee on the Effects of Atomic Radiation
USEPA	US Environmental Protection Agency
V	Vanadium
WHO	World Health Organisation.

XRD	X-Ray Diffraction
XRF	X-Ray Fluorescence
Zn	Zinc
Zr	Zirconium

PENILAIAN BAHAN ZARAH DAN KERADIOAKTIFAN BAWAAN UDARA DI QASSIM, ARAB SAUDI

ABSTRAK

Penyelidikan epidemiologi dan toksikologi telah menunjukkan hubungan rapat antara bahan zarah (PM) dengan gangguan pernafasan dan kardiovaskular. Justeru, PM di dalam udara yang kita sedut adalah memudaratkan kesihatan manusia. Banyak negara telah menjalankan kajian mendalam mengenai masalah yang berkaitan PM dan isu kesihatan dan alam sekitar. Walau bagaimanapun, terdapat kekurangan penyelidikan mengenai radioaktiviti, ciri fizikal dan kimia di dalam PM dari bandar Qassim, Arab Saudi. Oleh itu, kajian ini menerangkan pencirian radioaktiviti, fizikal dan kimia PM di Qassim. Penyelidikan ini memberi tumpuan kepada zarah radioaktif, yang seterusnya memberi kesan kepada komponen alam sekitar radionuklid yang berkaitan. Kepekatan zarah bersaiz kurang daripada 2.5 mikron dalam diameter aerodinamik (PM_{2.5}) dan Zarah Zarah kurang daripada 10 mikron dalam diameter aerodinamik (PM₁₀) telah diukur di dalam tempoh Julai 2020–Jun 2021 di kawasan bandar dan luar bandar Qassim. Di bandar Qassim, purata kepekatan PM masing-masing ialah 33.16 µg/m³ dan 155.38 µg/m³ untuk PM_{2.5}, dan PM₁₀. Di luar bandar Qassim, kepekatan PM masing-masing ialah 23.03 µg/m³ dan 93.57 µg/m³. Sebanyak 18 unsur telah ditentukan dan dikenal pasti, dan kepekataannya (mg/kg) dibandingkan dengan literatur. Tahap radioaktiviti semulajadi ²²⁶Ra, ²³²Th, dan ⁴⁰K dalam 276 sampel telah dinilai menggunakan pengesan natrium iodida Nal (TI). Kepekatan aktiviti Ra-226 adalah antara 10.01 hingga 47.60 Bq/kg dengan purata 350 ± 0.06 Bq/kg. Ke-232 adalah antara 11.30 hingga 44 Bq/kg, dengan purata 32 ± 0.4 Bq/kg. ⁴⁰K adalah antara 115.1 hingga 454.8 Bq/kg dengan purata 294.99 ± 1.31 Bq/kg.

Tahap bahaya sinar gamma dikira menggunakan pelbagai kaedah, termasuk setara Radium dengan purata 104.37 Bq/kg, indeks bahaya dalaman dan luaran dengan purata masing-masing 0.28 dan 0.38, dos yang diserap dengan purata 48.18 (nGy/ h), dos berkesan tahunan dengan purata 59.11 ($\mu\text{Sv/y}$), dan risiko seumur hidup dengan purata 4.14. Tambahan pula, sebuah Teknologi Penapisan Permeodinamik (PFT) telah dibangunkan yang telah menyumbang dengan cara yang menonjol dan inovatif kepada kajian penapisan PM di kawasan luar bandar. Penapis yang mampu menapis dan mengalih keluar PM tercemar secara kekal dari ruang luar di lokasi terpilih, sekali gus turut memanfaatkan ruang dalaman. Kos tahunan seunit aliran udara dikira \$162/tahun $\cdot\text{m}^3 \text{ s}^{-1}$. Kajian ini menggunakan dinamik bendalir pengiraan (SolidWorks) untuk menerangkan serakan PM di kawasan (1240 m \times 740 m) dan mensimulasikan penapis dalam makmal sebelum membangunkan penapis skala sebenar untuk percubaan lapangan.

ASSESSMENT OF AIRBORNE PARTICULATE MATTER AND RADIOACTIVITY AT QASSIM, SAUDI ARABIA

ABSTRACT

Epidemiological and toxicological research has shown a close connection between particulate matter (PM) with respiratory and cardiovascular disorders. Thus, PM in the air we breathe is detrimental to human health. Numerous nations have conducted in-depth study on the problem of PM and related health and environmental issues. Therefore, this study describes the radioactivity, physical and chemical properties of PM in Qassim. This research focuses on radioactive particle, which in turn impact the environmental compartments of the related radionuclides. PM of size less than 2.5 microns in aerodynamic diameter ($PM_{2.5}$) and PM less than 10 microns in aerodynamic diameter (PM_{10}) concentrations have been measured during the period of July 2020–June 2021 in the central urban and rural areas of Qassim. In urban Qassim, the average PM concentration were $33.16 \mu\text{g}/\text{m}^3$ and $155.38 \mu\text{g}/\text{m}^3$ for $PM_{2.5}$ and PM_{10} , respectively. In rural Qassim, the PM concentrations were $23.03 \mu\text{g}/\text{m}^3$ and $93.57 \mu\text{g}/\text{m}^3$, respectively. A total of 18 elements were determined and identified, and their concentrations in (mg/kg) were compared to literature. Natural radioactivity levels of ^{226}Ra , ^{232}Th , and ^{40}K in 276 samples were evaluated using sodium iodide (NaI) detector. Ra-226 activity concentration ranged from 10.01 to 47.60 Bq/kg with an average of 350.00 ± 0.06 Bq/kg. ^{232}Th ranged from 11.30 to 44 Bq/kg, with an average of 32.00 ± 0.40 Bq/kg. ^{40}K ranged from 115.10 to 454.80 Bq/kg with an average of 294.99 ± 1.31 Bq/kg. Gamma-ray hazard levels were calculated using a variety of methods, including the Radium equivalent with an average of 104.37 Bq/kg, internal and external hazard indices with an average of 0.28 and 0.38 respectively,

absorbed dose rate with an average of 48.18 (nGy/h), annual effective dose with an average of 59.11 ($\mu\text{Sv/y}$), and lifetime risk with an average of 4.14. Furthermore, a Permeodynamic Filtration Technology (PFT) developed has contributed in a prominent and innovative manner to the study of PM filtration in the outdoor urban areas. The filter was capable of permanently filtering and removing polluted and radioactive PMs from outdoor spaces at a selected location, thus also benefiting internal spaces. The annual cost per unit of air flow was calculated to be $\$162/\text{year}\cdot\text{m}^3\text{ s}^{-1}$. This work uses computational fluid dynamics (SolidWorks) to describe the dispersion of PM in an area ($1240\text{ m} \times 740\text{ m}$) and simulates the filter in the laboratory before developing the actual-scale-filter for the field trial.

CHAPTER 1

INTRODUCTION

1.1 Overview

Air pollution is a worldwide issue that is compounded by urbanization, traffic and industrial activity. High concentrations of tiny particles dispersed in ambient air are predicted to cause around 4 million premature deaths yearly, and levels of PM continues to grow globally (Shaddick et al., 2020; Prüss-Ustün et al., 2016).

Researchers have looked at two key sizes of PM, known as PM_{2.5} and PM₁₀. Long-term and short-term exposure to PM increases the chance of developing cardiovascular and respiratory diseases (Thurston et al., 2017). Human activities, such as the use of internal combustion engines for transportation, are a major contributor to the quantity of PM that is suspended in the air.

Standards for maximum quantities of airborne PM in the air have been set by the World Health Organization, and several national agencies have enacted legislative limitations in response to these guidelines (WHO, 2005; WHO, 2017). The WHO recommends that the maximum annual mean level of PM_{2.5} in the air should not exceed 10 µg/m³, however the regulatory annual mean quality level for PM_{2.5} in the European Union is 25 µg/m³. At the moment, 91 percent of the world's population lives in nations that do not meet the outdoor air quality guidelines set by the WHO (WBG, 2021). Some examples of these countries are Angola (32 µg/m³), Armenia (33 µg/m³), Bangladesh (61 µg/m³), China (53 µg/m³), India (91 µg/m³), and Peru (25 µg/m³) (WHO, 2018).

Multiparticle emissions are associated with a large proportion of radionuclides released by atomic activities, such as nuclear weapons testing, nuclear reactor explosions, and nuclear fire. In addition, radionuclides are found in particulate and

colloidal form in effluents from nuclear reactors and reworking plants under usual operational conditions. In the near area of nuclear waste dumped at sea, radioactive particles are also seen. The particulate composition and characteristics have been determined to be device-dependent after nuclear tests. The importance of studying radioactivity, chemical components and PM characteristics that lead to their poisoning has been emphasized by the Environmental Protection Agency (EPA) (Wyzga and Rohr, 2015; NRC, 2004). The more dangerous components of PM should be more efficiently targeted by the control regulations so that they could lower the risk of disease burden due to PM.

PM in the air, which may be of diverse sizes and contain both radioactive, chemical and biological components, is a primary subject of many research and regulations (Ali et al., 2019). When it comes to air pollutants, PM is responsible for the majority of disease burden, with more than 50% of the burden attributed to exposures to the environment that occur via inhalation (IHME, 2019). PM has recently been ranked sixth among the world's most significant health problems in terms of the sickness burden, and it is at the top of the list when it comes to environmental dangers (Cohen et al., 2017).

Regulation is an essential aspect of air quality management (Burns et al., 2020). To minimize radioactive and polluted PM emissions, a range of regulations and initiatives are being adopted and proposed. This is accomplished at the initial point of origin, for instance, by prohibiting or limiting the access of diesel-powered cars into metropolitan areas. The limitation is often determined by the emissions requirements of the vehicle, and it might vary from a complete ban to a charge for entering metropolitan areas (Hwang et al., 2016). Even in cities like Oslo, where cars are allowed in the downtown areas, parking on the streets has been severely limited, and

public access has emerged as one of the most important considerations in the planning and construction of new cities (Burch and Gilchrist, 2018). In addition to this, boosting the use of public transportation is another way to cut down on PM emissions (Hortensius et al., 2015). Using electric vehicles is another option to reduce particle pollution. Outdoor air filtration is an alternate method for lowering PM concentrations that has lately gained popularity among local authorities. Some cities throughout the world are implementing a wide range of technology to combat poor air quality in metropolitan areas. Beijing, Hong Kong, Delhi, and Bengaluru, for example, have all set aside huge sums of money to build outdoor air filtering systems. Smog Free Tower, a commercial application with an air filtering feature, has been deployed in numerous places in recent years (Nesterova and Danilovich, 2021). In 2018, the city of Xi'an in China constructed the world's largest air purifier, which stands at a height of 100 meters and claims to be able to filter the air across a 10 km² region (Cyranski, 2018). In September of 2018, the government of Delhi installed a total of 70 Wind Augmentation Purifying Units (WAYU). WAYUs were installed in Delhi, Mumbai, and Bengaluru; however, there are no operational details demonstrating the type of outdoor air filtration system used or the impact of using this technology to lower PM levels. This may be because there is a lack of information regarding the effects of using this technology to lower PM levels (Guttikunda and Jawahar, 2020). Bachler et al. (2021) conducted research to investigate the effect that outdoor air filters have on the particle concentration levels in an urban city in Germany that experiences high levels of traffic. According to the findings of yet another research carried out in Australia by Thomas et al. (2021), botanical biofilters have the potential to remove air pollutants caused by roadside traffic.

1.2 Scope of work

The three key research pillars that this thesis is built upon are (i) particle characterization with radioactive measurement and human health, (ii) polluted particle dispersion modelling in urban environments and (iii) filter design and testing. This thesis focuses entirely on PM collected in Qassim region from a variety of rural and urban areas. This is because the concentration of PM in this location is higher than the allowable amount of $25 \mu\text{g}/\text{m}^3$. As a consequence of this, it is vital to do research on the PM qualities in the target location in order to determine the kind of technology that is required to enhance the filtering system.

The Qassim region is located in the centre of Saudi Arabia. As in many other crowded cities across the world, rising pollution levels (over $25 \mu\text{g}/\text{m}^3$) in urban air quality are becoming a source of concern, particularly the effect of radioactive PM on human health and the environment. Many nations have tested the concentration of components in PM. More data on the key components of PM_{10} and $\text{PM}_{2.5}$ are needed in urban Qassim. Furthermore, there is no data to derive typical averages of chemical compositions.

In general, there are two types of radiation based on their occurrence: man-made radiation and natural radiation. People are always exposed to radiation due to the presence of natural radiation. In the world's ecosystem, natural radioactivity is widely dispersed. Including the soil, plant, water, air, coal and phosphate are presented. Natural soil radioactivity is largely produced from the ^{238}U , ^{232}Th and ^{40}K family series. Natural radioactive materials (NORMs) in the soil are elements of external exposure to gamma-rays to which people are frequently exposed. In this study, the focus was to measure natural radionuclides in 276 samples of PM in Qassim region. The activity concentration for Ra-226, Th-232 and Ra-226 was estimated.

Furthermore, Gamma-ray hazard levels were determined using a number of methodologies, including the Radium equivalent, internal and external hazard indices, absorbed dose, annually effective dose, and lifetime risk.

To address the issue of radioactive airborne PM and the characteristics of airborne PM, a novel filter has been created that is capable of efficiently lowering radioactive and polluted PM concentrations while simultaneously improving air quality by reducing the PM concentration. The cost-effectiveness of the filtering system as well as the reduction of expenditures incurred during production and operation are of primary concern. The development and evaluation of filters included the use of both computational and experimental methods, with the former taking place in a laboratory setting while the latter involved field testing. The purpose of the experiment in the laboratory is to study the effectiveness of permeodynamic PM-filtering in an indoor environment, that has less changeable components than an outdoor environment. In order to carry out this experiment successfully, it need a suitable laboratory as well as a filter that has been correctly designed and constructed. The inside filter measured 2 meters in length, 1.5 meters in height, and 0.12 meters in width, while the outdoor filter measured 3 meters in length, 2 meters in height, and 0.16 meters in width. The filter for the laboratory experiment was examined prior to analyzing the outdoor filter in order to identify the best filter material for the outdoor experiment and achieve optimal filter performance.

Computational Fluid Dynamic can analyze environmental challenges in both indoor and outdoor settings. The distribution of PM in urban and neighborhood regions has been modelled in this study. The computational domain for this experiment took the shape of a rectangle and had the following dimensions: 1240

meters in length, 740 meters in width, and 200 meters in height (Union Street and King Street). The information that was acquired is shown via animations and still photos.

1.3 Problem Statement

Outdoor radioactive PM pollution is one of the most serious environmental issues today. PM sources in metropolitan areas include both human and natural sources (Allen et al., 2001; Bilos et al., 2001; Wang et al., 2005). PM pollution in cities has been related to a number of acute and chronic health effects (WHO, 2014; WHO, 2017). It is essential to emphasize that the levels of airborne PM pollution in cities and towns have exceeded critical levels, which has a severe effect not only on the economy but also on human health and the environment (Selokar et al., 2020). The annual levels of airborne PM pollution continue to rise despite the levels of control that are in place and the gains that have been made in the management of PM emissions (Longhurst, 2016). The hazard of PM is determined by its source (Tsiouri et al., 2015). When radioactivity is taken into consideration, the hazard become more serious (Nyhan et al., 2019). Natural pollution episodes like desert dust and sea spray are often only reported at times when there is advection. Following even brief exposures to ionizing radiation, there is a higher likelihood of developing lung disorders and experiencing death, according to findings from previous research (UNSCEAR, 2000). Although ambient PM has been linked in a way that can be reproduced to impaired lung function and to increased morbidity due to respiratory issues (Kelly and Fussell, 2011), the sorts of toxic PM are not completely understood (Franchini and Mannucci, 2007; Riedl, 2008). As a result of this, the study analyzed the effects of the radioactivity measurement on human health and conducted an investigation into the radioactivity of PM. The research will also look at a novel way to solve the problem of radioactive and airborne PM pollution by employing a large-

scale outdoor permeodynamic filter. This filtering system's applicability might be beneficial in regions such as street canyons, bus stops, smart cities, and underground railways. Through this study, an effort will be made to enhance the operational and environmental benefits of filters as well as their service life. The benefits may be expanded to cover a larger area, such as a town or region. The overall benefits of PM filtration exceed the costs involved, for example, if morbidity and mortality rates can be brought down, healthcare costs may become more manageable.

1.4 Objectives of the research

1. To determine the radioactivity, physical, and chemical components of PM at a selected location in Qassim;
2. To investigate distribution of PM at a representative street canyon selected;
3. To execute a simulation of a small-scale filter in the laboratory using SolidWorks prior to producing an actual field experiment size filter;
4. To design and fabricate a new filter and conduct laboratory tests on a small scale as well as restricted field experiments at the places of interest in order to evaluate the effectiveness of the PFT of removing polluted and radioactive PM.

1.5 Outline of thesis

This thesis is divided into five chapters. Chapter 1 contains an introduction to the entire thesis, outlining the problem statement, aims, and scope of research. Chapter 2 examines a wide range of studies that are pertinent to this thesis study. Chapter 3 describes the materials and procedures used in the experimental component of this thesis study. Chapter 4 contains the obtained results and discussions. The conclusion and recommendations for further investigation are summarized in Chapter 5.

CHAPTER 2

LITERATURE REVIEW

2.1 Particulate Matter on urban environment

Airborne PM pollution can cause or exacerbate respiratory problems and is a crucial factor in the transmission of infectious, neurological, viral, and allergy diseases (Bernstein et al., 2004; Finlayson-Pitts, 1997; Hinds, 1999). PM plays an important role in the climate system and has an impact on ecosystem health, human health, and air quality (IPCC, 2013).

Measurements of airborne particle concentrations and dispersion have been made in a number of cities, including those in Korea, China, India, and the UK (Ny and Lee, 2011; Beddows, 2015; Fang et al., 2008; Khillare and Sarkar, 2012). On the other hand, Qassim lacks data on PM_{2.5} and PM₁₀ concentrations.

The total prevalence rate of non-communicable illnesses was found to have increased significantly in recent research of the Qassim region. Over the years 2011 and 2015, the percentage increased to 15.7% from 7.1%. Diseases of the cardiovascular system, problems of the skin and eyes, impairments of hearing and vision, diabetes. Air pollution with a significant amount of PM in the air are blamed for the rise in diseases (Mustafa et al., 2016). As the frequency of sandstorms rises, these health issues get worse. Sandstorm occurrences have increased as a result of low-pressure systems in the north of Qassim in the spring. Cold fronts that are moving toward the southeast are causing sandstorms in such low-pressure zones. Dust particles are dispersed as a result of the approaching 20 km/h horizontal wind speed. Most dust storms are brought on by velocities of more than 35 km/h.

The physical and chemical characteristics of the atmosphere are significantly influenced by crustal aerosols, which are made up of deposits from canyons and

deserts. Recently, this crucial function has become more thoroughly appreciated, and several studies on the impacts of desert aerosols on the atmosphere have been conducted (Rahn et al., 1979). The majority of the components found in the airborne PM are found in the crust and may have a soil origin. Even in the most distant areas of the temperate and polar zones, it's possible that deserts constitute the primary source of this crustal dust (Al-Taani et al., 2015). In the troposphere, large quantities of aerosol components are mostly traced to their crustal sources (Chan et al., 1997).

Anthropic aerosols are produced by industrial pollutants, energy production, and agricultural practices. Over the course of the last several decades, researchers have shown an interest in investigating the metal concentrations of dust as well as the effects that dust aerosols have on the surrounding environment; the survey's results showed a rise in PM contamination within a short time (Amato et al., 2009; Doronzo and Al-Dousari, 2019). Regarding atmospheric particle pollution, the chemical makeup of PM, which is crucial in producing negative health and environmental effects in metropolitan areas, is of major public concern. These PM concentrations contain particles with a range of shapes, sizes, thermodynamic properties, and chemical compositions (AQEG, 2005, 2012; Fromme et al., 2008).

The capacity of PM to transit across atmospheric countries and continents, as well as its influence on global warming, necessitates PM classification by governments, regulators, and academics (Dockery et al., 1993; Salazar et al., 2012). The PM in the environment is not simply a single pollutant but rather a diversity of chemical species, which may include traces of metals, carbon in its elemental form, nitrate, sulfate, and a wide range of organic compounds (Fraser, 2003).

The stationary testing facilities run by government organizations for regulatory purposes often measure the chemical components of PM. In the United States, for

example, the Interagency Monitoring of Protected Visual Environment and the United State Environmental Protection Agency Chemical Network are the primary PM chemical monitoring equations used to estimate the chemical components. However, there is no data accessible in Qassim, Saudi Arabia, due to the fact that tracking networks do not conduct analysis on the chemical components. As a result, this investigation has a primary focus on the levels of PM₁, PM_{2.5}, and PM₁₀ in rural and urban areas of Qassim, Saudi Arabia.

Tiny solid and liquid particles suspended in a gaseous medium make up an aerosol (Hinds, 1999). Typically referred to as PM, these samples of particle aerosols have sizes varying from nanometers (nm) to micrometers (μm). The United Kingdom Air Quality Standards Regulations, 2010, define PM₁₀ as PMs that passes over a size-selective inlet with a 50% efficiency cut-off at an aerodynamic diameter of 10 μm (EN 12341); PM_{2.5} is the PMs size that passes over a size-selective inlet with a 50% aerodynamic diameter efficiency cut-off at an aerodynamic diameter of 2.5 μm (EN 14907). The amount of PMs in one cubic meter of air is measured and recorded as PM mass, which is often measured in micrograms per cubic meter, $\mu\text{g}/\text{m}^3$.

Monitoring and research into the chemical and physical characteristics of airborne particles are crucial because they have an impact on the environment. Researching the characteristics of PM, such as its chemical make-up and size distributions, among other aspects, will yield essential information that may be used to understand the procedures and sources that lead to the formation of atmospheric aerosols.

2.1.1 Categories of particulate matter

PMs is one of the main airborne contaminants in cities (Harrison, 2003). Airborne PM, which is produced from a variety of sources such as main automobile

exhaust, industrial combustion and mechanical operations, and gaseous pollutants, contains a complex mixture of organic and inorganic materials (Gartrell and Friedlander, 1975). Particles can be categorized in a variety of ways, such as primary and secondary particles, which are based on how they form. While secondary particles are created by the gas-to-particle conversion of precursor gases in the atmosphere, prominent particles are released directly into the environment (Vallius, 2005). The geographical area, atmospheric chemistry, and the mix of emissions, all have a significant role in determining the relevance of primary versus secondary elements. For instance, Scotland's $PM_{2.5} / PM_{10}$ ratio dropped to below 0.6, which is consistent with the UK's increased contribution of secondary particles from the region's south-eastern nations (Harrison et al., 2012).

Significant PM gradients have been seen between rural, urban, and road sites, particularly in crowded street canyon locations. According to studies conducted at these locations, $PM_{2.5}$ levels are highest in winter and lowest in summer, it is consistent with increased mixing or volatilization when high-temperature semi-volatile compounds are present. (Harrison et al., 2012). PMs may travel from locations with high emissions to comparatively pristine remote places.

2.1.1.(a) Primary particulate matter

The primary particles released are of various sizes. During fuel combustion, aerodynamic particles smaller than 1 μm are frequent. Particles with an aerodynamic size greater than 10 μm , that are less important in PM, are often located on the surface for a short time span. Primary PMs have several origins, including mobile and stationary sources. Road transportation is the primary mobility source, and it generates both small and large PM (from brake wear and pneumatic). Examples of stationary sources include burning fuel for home, commercial, and agricultural purposes. Additionally, many primary particles come from important natural sources, including seawater and biogenic materials like pollen fragments.

2.1.1.(b) Secondary particulate matter

Chemical processes that gas precursors release into the atmosphere produce secondary PM. The main precursory emissions are produced by motor vehicles, domestic wood burning, and activities like preparing meat, which release extremely complex mixtures of organic and inorganic substances into the gaseous and particle phases. In meteorological conditions, secondary particle production is time-dependent on the characteristics of their precursors. Then, it takes hours or days for the PM to spread to neighboring locations.

According to Dockery and Pope (1997) and Kim (2015), PMs are a combination of suspended air particles that can be liquid or solid, and their structure varies depending on the atmospheric environment and source of the PM (Pöschl, 2005). Urban PM primarily contains parts of primary and secondary particulate contaminants (Eatough et al., 2003). These studies—Harrison et al. (1999), Pöschl (2005), and Chu et al., (2004)—present the important characteristics of PM.

Inorganic mass such as sulphate, which is shaped by the oxidation of sulfur dioxide in the air, ammonium, which is produced when atmospheric ammonia reacts with sulfuric and nitric acids to produce ammonium salts, and nitrate, which is predominantly produced through nitrate oxidation (NO and NO₂). PM is mostly created by humans, such as PM from diesel automobiles, power plants; refineries, chlorine created mostly by sea spray. Carbon emissions from burning include mass-elemental carbon particles. Concentrated or adsorbed organic mass-hydrocarbons, examples include well-known human carcinogens like polycyclic aromatic hydrocarbons and hydrocarbon compounds. Materials made of crustaceans: These materials mostly depict the local geology or environment, including surface layers, ground-up materials, and wind-driven habitats. Semi-volatile species encompass a variety of species, including nitrates from ammonia, bound water, and organic semi-volatile compounds. These species mostly occur in the atmosphere, existing both as gases and as PM. Biological components include spores, pollen, bacteria, and plant fragments.

2.1.2 Airborne particulate matter physical characteristics

PM in the air has a variety of features, each of which contributes significantly to the function it plays in the process of the atmosphere. Researchers have looked at their population sizes, masses, dimensions, chemical make-up, as well as their aerodynamic and optical properties (Finlayson-Pitts and Pitts, 1986). The size of the particles is the most crucially essential physical characteristic, particularly for PM_{2.5} and PM₁₀. The size of the particles reveals the origin of the particles and is related to the impacts that the particles have on one's health via the light-dispersing qualities that they possess, among other effects that include those on climate and aesthetics. The size of particles may vary anywhere from 0.002 microns to 100 microns, however the particles with dimensions between 0.001 and 10 microns are considered to be the most

fundamental in the study of the chemistry and physics of the atmosphere. The effective diameter, which relies on a physical characteristic rather than a geometrical one, is another attribute that reflects scale. The most common effective diameter is the aerodynamic diameter, which is denoted by "D_p," and the diameter of unit density, which is denoted by "g," both of which have the same flow rate as the measurement particle (Hinds, 1999). For instance, a particle with an aerodynamic diameter of one micrometer shares the same inertial characteristics as a sphere with a diameter of one micrometer and a mass of one m⁻³, despite the fact that the actual size is different.

Figure 2.1 illustrates how tiny these particles are. Since the hair is 50 μm in diameter, the PM_{2.5} is around 1/20 in width and the PM₁₀ is 1/5 in width.

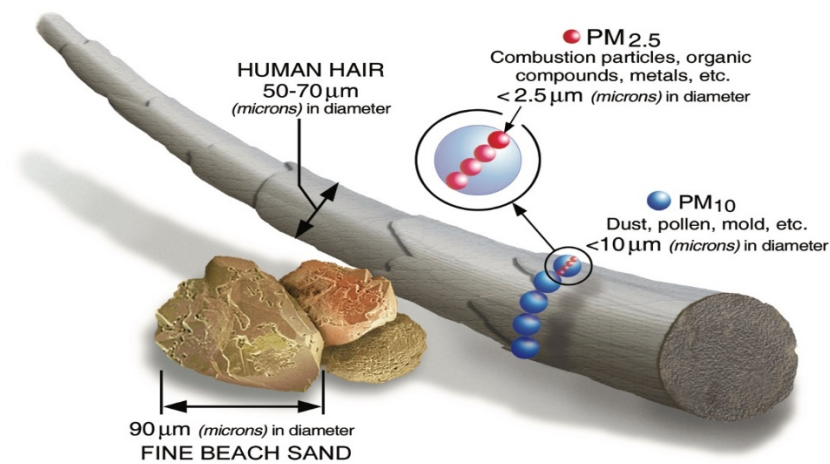


Figure 2.1: Size comparisons for PM particles (USEPA, 2022).

For the purposes of the most recent measurements of the atmosphere, PM can be separated into the following three categories: PM₁₀, PM_{2.5}, and PM_{2.5-10}, as well as PM_{0.1}, these particles have the potential to cause significant harm to the lungs and have an effect on the respiratory system (Pakkanen et al., 2001). The Whitby trimodal model was developed by Whitby (2007). This model is a more straightforward representation of the size distribution due to the formation process. This model showed

that the change from aerosol number distributions to volume distributions exhibits three phases, which are called nucleus modes, accumulation modes, and ground modes, respectively. D_p was less than 0.1 μm in nucleation modes, between 0.1 and 1.0 or 2.0 μm in aggregation modes, and more than 1.0 or 2.0 μm in coarse types (Figure 2.2). In every model, a lognormal feature was used to represent the data. There are two components that make up the nucleation mode: the nucleation mode and the Aitken mode. According to the findings of the vast majority of studies, the nucleation mode is far less than the Aitken mode. As a result, the nuclear mode has an upper limit of around 0.02 to 0.03 μm , while the Aitken mode is significantly bigger (Jaffrezo et al., 2005; Pakkanen et al., 2001). Whitby divided the particles into two primary cracks, one for fine particles with diameters of less than 1.0 or 2.0 μm and the other for coarse particles with sizes of more than 1.0 or 2.0 μm . The legislative air quality objectives for PM_{10} and $\text{PM}_{2.5}$ are currently defined as the percentages of particles with an aerodynamic diameter of less than 10 and 2.5 micrometers, respectively. This both represents and modifies the nucleation mode, also known as the Aitken mode, which has a diameter of less than 0.1 μm , the accumulation mode, which has a diameter ranging from 0.1 to 2.5 μm , and the coarse mode, which has a diameter ranging from 2.5 to 10 μm . Two frequent categories for fine particles are the small fractions (with a D_p of less than 2.5 μm) and the ultrafine fractions (with a D_p of less than 0.1 μm).

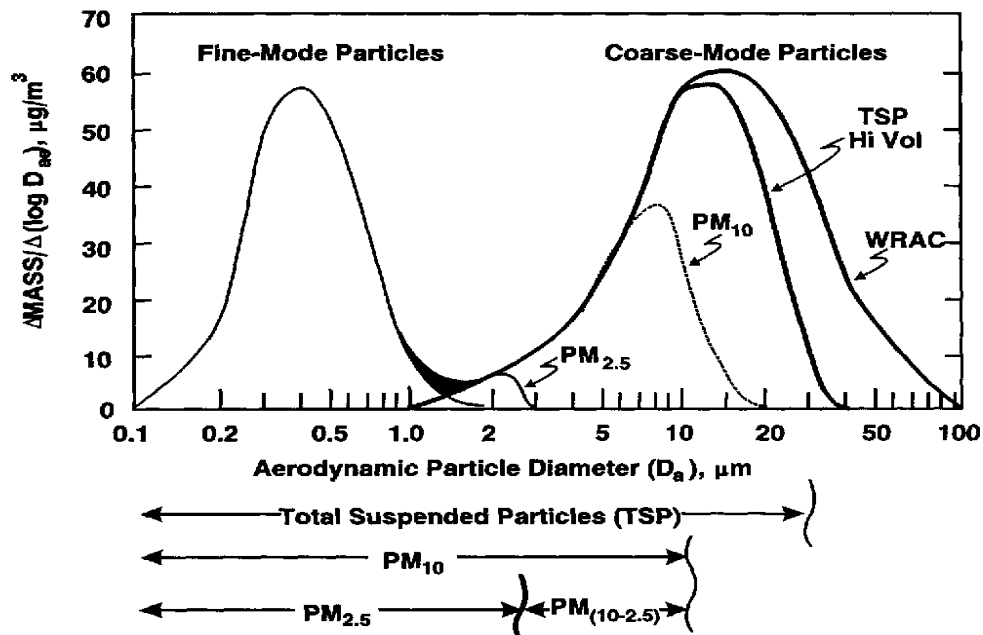


Figure 2.2: Schematic display of the distribution of PM size in ambient air (USEPA, 1996).

The scale distribution of aerosol particles changes throughout the environment due to the formation of new particles (gases to conditions by photochemical substrate oxidation), eventual growth (condensation and coagulation), degradation and evaporation (diminution, diffusion, impaction, and precipitation) (Hinds, 2001). Coagulation and particle surface condensation reduce the sample scale. When more vapors molecules are present on the outside of the PMs, condensation takes place, increasing the aerosol's phase after particle impact. The opposing action, evaporation, alters the bulk and leads to net molecular loss and a decrease in PM.

Particles in the fine and coarse modes have different sizes, origins, elimination processes, chemical, physical, and biological properties. It is common for the finely modified particles to originate directly from combustion, to develop as secondary particles from combustion sources, or to come into being as a result of the process of gas condensation or the processes of coagulation and adsorption. Although bigger

PMs might develop locally by mechanical destruction, breakdown (ocean spray), manufacturing activity, or the re-dispersion of surface matter, especially under dry circumstances, particles are frequently associated with long-distance transit in the fine mode. In metropolitan settings, automobile traffic emissions are the main source of fine PM. Untreated particle matter mostly originates from pollution, resuspended surface powders, and coastal pulverization. (QUARG, 1996).

2.1.2.(a) Normal and Logarithmic Normal Distributions

A dependent variable may be distributed according to the lognormal distribution, which is a formula in a normal or Gaussian way on the logarithmic scale of a different variable. This function has been used for a while to categorize the size of particles in atmospheric aerosols. This functional relationship was utilized by Heintzenberg (1994) to define the optical aerosol characteristics. Whitby (1974) used this method to construct a broad idea of the multi-modal presence of atmospheric aerosols by integrating three log-normal distributions. The specifics of three different distribution moments were also incorporated into the log-normal modelling of the experimental results.

The impacts of lognormal techniques are employed in modelling clouds, aerosols, and precipitation, as well as comparing the results to actual data (Heintzenberg, 1994). Consider the normal distribution as one possible particle distribution in Equation 2.1.

$$n(r) = \frac{N_0}{\sqrt{2\pi}} \frac{1}{\sigma_0} \exp \left[-\frac{(r-\mu_0)^2}{2 \sigma_0^2} \right] \quad (\text{Equation 2.1})$$

where μ_0 represents the distribution's mean and σ_0 represents the SD of the sample. An aerosol's PM size often comprises numerous magnitude orders. As a result, the SD of the normal distribution fit of observed PMs sizes is relatively large. Because

negative radii are permissible, the typical diversion is likewise unfavourable. Particle radius logarithm distributions, which are normally distributed, provide a better characterization of aerosol distributions. Let $l = \ln(r)$ in Equation 2.2.

$$n_l(l) = \frac{dN(l)}{dl} = \frac{N_0}{\sqrt{2\pi}} \frac{1}{\sigma} \exp\left[-\frac{(l-\mu)^2}{2\sigma^2}\right] \quad (\text{Equation 2.2})$$

where the average and SD, of $l = \ln(r)$ are given in Equation 2.3 and 2.4.

$$\mu = \frac{\int_{-\infty}^{\infty} l n_l(l) dl}{\int_{-\infty}^{\infty} n_l(l) dl} = \frac{1}{N_0} \int_{-\infty}^{\infty} l n_l(l) dl \quad (\text{Equation 2.3})$$

$$\sigma^2 = \frac{1}{N_0} \int_{-\infty}^{\infty} (l - \mu)^2 n_l(l) dl \quad (\text{Equation 2.4})$$

In terms of radius, the lognormal distribution is commonly stated (Equation 2.5). It should be noted:

$$\frac{dl}{dr} = \frac{1}{r} \quad (\text{Equation 2.5})$$

The radius is then obtained instead of the log radius (Equation 2.6) (Grainger 2012).

$$n(r) = \frac{dN}{dr} = \frac{dN(l)}{dl} \frac{dl}{dr} = n_l(l) \frac{dl}{dr} = \frac{N_0}{\sqrt{2\pi}} \frac{1}{\sigma r} \exp\left[-\frac{(\ln r - \mu)^2}{2\sigma^2}\right] \quad (\text{Equation 2.6})$$

The geometrical norm difference, S , is frequently used to express the distribution spread. From this definition, the lognormal standard deviation S should be larger than or equal to one. When S equals one, the distribution is monodispersed. S values in typical aerosol distributions vary from 1.5 - 2.0.

Perhaps the most common form of the lognormal distribution seen in atmospheric science literature is the one obtained by combining the parameters r_m or μ and σ or S (Equation 2.7) (Grainger, 2012).

$$n(r) = \frac{N_0}{\sqrt{2\pi}} \frac{1}{\ln(S) r} \exp\left[-\frac{(\ln r - \ln r_m)^2}{2 \ln^2(S)}\right] \quad (\text{Equation 2.7})$$

A Gaussian distribution's particle number density expressed in units of log (radius) is shown in Figure 2.3. Additionally, shown in the picture is the particle density distribution plotted against unit radius. The median, mean, or mode in log

space equals the natural logarithm of linear space, and the field is maintained throughout transformation.

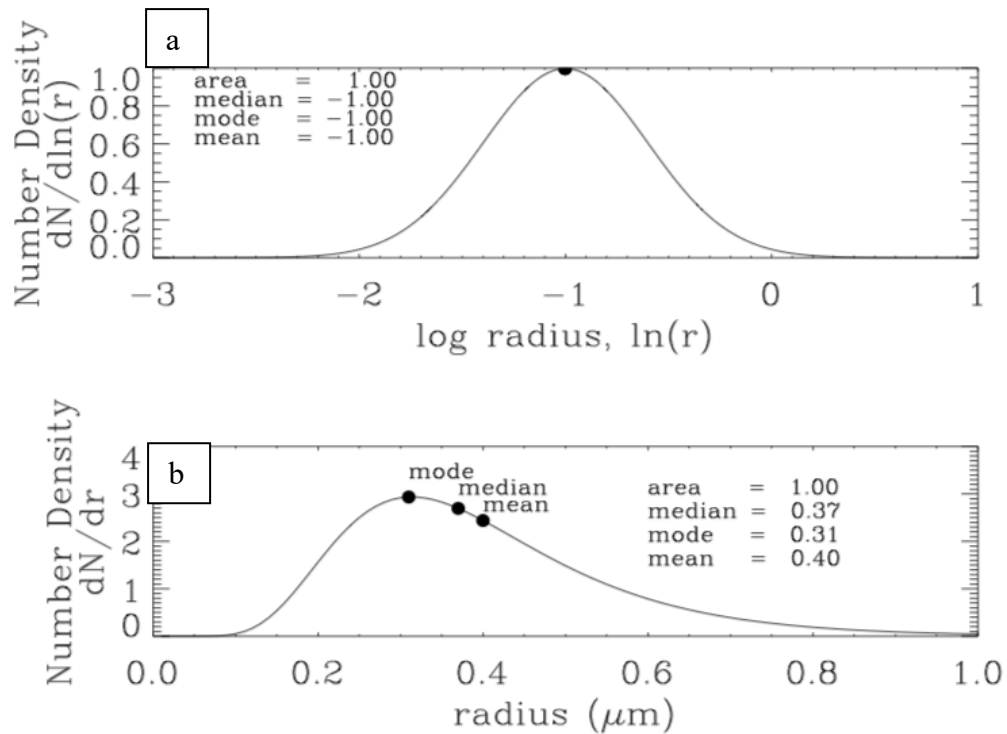


Figure 2.3: Log-normal distribution plotted in log space (a) with parameters $N_0 = 1$, $\mu = -1$ and $\sigma = 0.4$ and linear space (b); The distribution mode, median and mean in log and linear space, respectively (Grainger, 2012).

The majority of airborne particle size distributions do not lend themselves to normal distribution statistics (aerosol). According to O'Neill et al. (2000), lognormal distributions are often better matched and serve as better standards for aerosols. The fact that the particle size distributions are log normal is just the best fit experimentally; there is no specific scientific rationale behind it. When mathematical analysis is applied to the size distributions of aerosol particles, it consistently relies on lognormal distributions (TSI, 2012).

2.1.2.(b) Shape of particulate matter

Particulates can take on numerous shapes, such as circular (fly ash), crystalline (sea salt) or irregular (crust), asbestos, as well as different morphologies, including oil burning particulates, dense (crystal), core or accumulated (vehicle exhausts) (Sabbioni and Zappia, 1993; Sheridan et al., 1993; DeBock et al., 1994; Yao et al., 2010; Nieder et al., 2018). Vapor condensation, evaporation, and coagulation are just a few of the processes that can cause these particles to alter in morphology and structure (Tahir et al., 2008).

Chemical interactions and reactions often influence particle structure during transit from their origin to receiving locations. These mechanisms are responsible for the formation of three distinct kinds of particle structures: exterior particles of composition; particles that do not mix (such as fly ash, crystal, and sea salt PM), and internal particles of composition (Tsay et al., 1991; Bondy et al., 2018); PM in the internal system, which includes particles with non-uniform component mixings, such as soot particles, sea-salt, or crustacean (Pakkanen, 1996; Archer et al., 2021; Tsay et al., 1991).

Studies of PMs structure are a relatively new scientific field (Colbeck et al., 1997-2010; Dormann and Fiorani, 2012). A wide range of approaches have been employed to establish the size, basic components of PMs and structure (Wilson et al., 2002). These approaches, however, do not give information on particle structure through specific proportions and forms. These kinds of findings are attainable via the use of scanning electron microscopy in conjunction with an energy dispersion Spectroscopy (Paoletti et al., 2002; Xie et al., 2004; Patio et al., 2019).

2.1.3 Airborne particulate matter chemical characteristics

In order to improve the quality of the air that people breathe in the world, it is necessary to measure the chemical components that comprise PM_{2.5} according to the

Directive of the European Parliament and of the Council on May 21, 2008 (2008/50/EC). The measures are designed to guarantee that appropriate knowledge of the background circumstances is available, as required by the Directive. In PM_{2.5} estimates, the total mass quantities as well as the amounts of important chemicals to define their compounds should be considered. At the very minimum, Nitrate, Sulfate, Sodium, Potassium, Calcium, Ammonium, Chlorine, Magnesium, and organic Carbon dioxide should be tested. The data is essential for understanding specific pollutants, analyzing the possible effects of long-range air emissions transport, determining the higher rates of harmful PM in inhabited regions, and conducting source delivery studies and understand PM pollutants.

Fossil fuel combustion (mainly in mining, vehicles, and power production) is the main contributor of anthropogenic Nitrogen dioxide (Graedel et al., 1995; He et al., 2014). The increase in biosphere nitrogen has resulted in a significant change in the biodiversity, soil acidity, water quality, and fertilizer status of soils (Ho et al., 2004; Stewart et al., 2021). These findings show that metropolitan settings pay special attention to VOCs, such as toluene, benzene, and xylene, which typically result from automobile emissions (Kerchich and Kerbachi, 2012).

Chromium, Lead, Nickel, Zinc, Cadmium, and Copper are examples of anthropogenic tracer plots, while Ca, Mg, K, Na, Iron (Fe), and Aluminium (Al) are examples of earth surface elements or tracer plots. Depending on the place of origin and the climate there, some components may be classified as either originating from natural or partly human causes (Wang et al., 2006). Metal PMs are produced by a variety of human and natural sources and are found in urban ambient air. In contrast to natural sources such as forest fires, sea salt spray, sand blown in by the wind, and volcanic activity, manmade sources include burning fossil fuels, burning wood,

producing electricity, building construction, and burning garbage (Bilos et al., 2001; Wang et al., 2005; Nagar et al., 2014).

Significant vehicle emissions of the elements Cr, Cu, Pb, Cd, Zn, and Fe have been found as indicators for a variety of atmospheric origins, including resuspended dust and soils, which include the elements Ca, Al, Mg, and Fe (Kong et al., 2011; Salvador et al., 2004; Sternbeck et al., 2002). Increased levels of metals like Cu, Cd, Zn, and Ni may result from certain industrial metallurgical operations (Bilos et al., 2001; Wang et al., 2005; Torres et al., 2012). For example, Zn and K are released during industrial processes (Allts et al., 2001; Marcazzan et al., 2001; Taiwo et al., 2014); K, Zn, and Pb are released during incinerators (Funasaka et al., 2003); Cr and Fe are released during coal combustion (Gao et al., 2002); Ni is released during oil combustion; and Al and Fe are released during construction (Taiwo et al., 2014; Espinoza et al., 2001; Chao and Wong, 2002). These elements Mg, Ca, Al, K, and Fe are frequently found in crustal sources including industrial and agricultural processes, construction projects, and paved and unpaved roadways. Na is more often used to identify salt particles (Lynch, 1991; Manders et al., 2010). A strong chloride interaction in marine aerosols may be the cause of Mg. An enhanced association among Ca and the tracer for diesel exhaust is used to support the idea that Ca might have both natural and anthropogenic origins (Harrison et al., 2004; Charron et al., 2019).

The chemical makeup of airborne PM has been the subject of various earlier studies (Chow et al., 1994; Eldred et al., 1997; Yin and Harrison, 2008; Ding et al., 2019). This finding suggests that multiple components exist in the structure of PM and are influenced by environmental chemical reactions, emissions, long-scale transport effects, and meteorological variables.

Airborne particles contain both the primary and minor elements of PM. Harrison and Yin (2000) examined the proportional distribution of significant chemical elements known as "bulk chemical composition" in metropolitan regions in the UK and compared them to global situations. The main components of dust include crustal sources, biological materials, SO₄, NO₃, NH₄, Cl, Elemental carbon (EC), and Organic Carbon (OC). The many small chemical components of airborne particles affect the analytical techniques' sensitivity and detection limits for respective concentrations. These small components, which include trace metals like Cd, Pb, Ni, Mercury (Hg), Zn, Cr, and Manganese (Mn), are employed into chemical and metallurgical methods. Even though they only include a tiny fraction of the overall mass of organic compounds, these components play a crucial role in the collection of organic molecules. Table 2.1 displays the PM composition measurements and fluctuations in component concentrations at several locations throughout the world, exhibiting notable temporal variability in PM chemical levels. In Europe, Putaud et al. (2010) have compiled information on the chemical properties of PM collected over the past ten years from European Aerosol Research at kerbside, rural and urban locations. In Table 2.2, the findings for PMs are displayed.

Querol et al. (2007) looked at the levels of PM_{2.5} and PM₁₀ in 33 locations (rural, urban, and agricultural) in Spain. For Mn, Cr, Cu, Arsenic (As), Zn, Tungsten (W), Tin (Sn), Ni, Cesium (Cs), Vanadium (V), and Pb, the average concentrations of these trace elements were greater in industrial settings than in rural ones. High levels of selenium (Se), Sn, Cr, Mn, Zn, Ni, Molybdenum (Mo), Cadmium (Cd), and Pb were linked to the manufacturing of steel, whereas copper metallurgy zones showed substantial Cu, As, Bismuth (Bi), and Gallium (Ga) levels. High amounts of Lithium (Li), Pb, As, Zirconium (Zr), Se, Cs, Titanium (Ti), and Cobalt (Co) were associated

with the manufacturing of glazed ceramics, whereas low levels of Zn and Cd suggested zinc metallurgy. High quantities of Ni and V were found in the traces left behind by petrochemical factories and/or the burning of fuel oil. As a result of traffic pollution (tyre and brake abrasion), there was also a relatively large level of Cu-Sb and Zn-Ba in metropolitan areas.